




Whole-body MRI in oncology: can a single anatomic T2 Dixon sequence replace the combination of T1 and STIR sequences to detect skeletal metastasis and myeloma?

Ophelye Chiabai¹ · Sandy Van Nieuwenhove¹ · Marie-Christiane Vekemans² · Bertrand Tombal³ · Frank Peeters¹ · Joris Wuts^{1,4} · Perrine Triqueneaux¹ · Patrick Omoumi⁵ · Thomas Kirchgesser¹ · Nicolas Michoux¹ · Frédéric E. Lecouvet¹ 

Received: 9 February 2022 / Revised: 21 June 2022 / Accepted: 30 June 2022 / Published online: 4 August 2022
© The Author(s) 2022

Abstract

Objectives To compare the diagnostic accuracy of a single T2 Dixon sequence to the combination T1+STIR as anatomical sequences used for detecting tumoral bone marrow lesions in whole-body MRI (WB-MRI) examinations.

Methods Between January 2019 and January 2020, seventy-two consecutive patients (55 men, 17 women, median age = 66 years) with solid (prostate, breast, neuroendocrine) cancers at high risk of metastasis or proven multiple myeloma (MM) prospectively underwent a WB-MRI examination including coronal T1, STIR, T2 Dixon and axial diffusion-weighted imaging sequences. Two radiologists independently assessed the combination of T1+STIR sequences and the fat+water reconstructions from the T2 Dixon sequence. The reference standard was established by consensus reading of WB-MRI and concurrent imaging available at baseline and at 6 months. Repeatability and reproducibility of MRI scores (presence and semi-quantitative count of lesions), image quality (SNR: signal-to-noise, CNR: contrast-to-noise, CRR: contrast-to-reference ratios), and diagnostic characteristics (Se: sensitivity, Sp: specificity, Acc: accuracy) were assessed *per*-skeletal region and *per*-patient.

Results Repeatability and reproducibility were at least good regardless of the score, region, and protocol ($0.67 \leq AC1 \leq 0.98$). CRR was higher on T2 Dixon fat compared to T1 ($p < 0.0001$) and on T2 Dixon water compared to STIR ($p = 0.0128$). In the *per*-patient analysis, Acc of the T2 Dixon fat+water was higher than that of T1+STIR for the senior reader (Acc = +0.027 [+0.025; +0.029], $p < 0.0001$) and lower for the junior reader (Acc = -0.029 [-0.031; -0.027], $p < 0.0001$).

Conclusions A single T2 Dixon sequence with fat+water reconstructions offers similar reproducibility and diagnostic accuracy as the recommended combination of T1+STIR sequences and can be used for skeletal screening in oncology, allowing significant time-saving.

Ophelye Chiabai and Sandy Van Nieuwenhove equally contributed to the study.

Nicolas Michoux and Frédéric E. Lecouvet equally contributed to the study.

✉ Frédéric E. Lecouvet
frederic.lecouvet@uclouvain.be

¹ Department of Radiology and Medical Imaging, Cliniques Universitaires Saint Luc, Institut de Recherche Expérimentale & Clinique (IREC), Université Catholique de Louvain (UCLouvain), Hippocrate Avenue, 10, B-1200 Brussels, Belgium

² Department of Internal Medicine, Hematology Unit, Cliniques Universitaires Saint Luc, Institut de Recherche Expérimentale & Clinique (IREC), Université Catholique de Louvain (UCLouvain), Brussels, Belgium

³ Department of Surgery, Urology Unit, Cliniques Universitaires Saint Luc, Institut de Recherche Expérimentale & Clinique (IREC), Université Catholique de Louvain (UCLouvain), Brussels, Belgium

⁴ Department of Electronics and Informatics (ETRO), Vrije Universiteit Brussel, Brussels, Belgium

⁵ Department of Radiology, Centre Hospitalier Universitaire Vaudois (CHUV), Lausanne, Switzerland

Key Points

- Replacement of the standard anatomic T1 + STIR WB-MRI protocol by a single T2 Dixon sequence drastically shortens the examination time without loss of diagnostic accuracy.
- A protocol based on fat + water reconstructions from a single T2 Dixon sequence offers similar inter-reader agreement and a higher contrast-to-reference ratio for detecting lesions compared to the standard T1 + STIR protocol.
- Differences in the accuracy between the two protocols are marginal (+ 3% in favor of the T2 Dixon with the senior reader; – 3% against the T2 Dixon with the junior reader).

Keywords Magnetic resonance imaging · Whole-body imaging · Cancer · Metastasis · Multiple myeloma

Abbreviations

AC1	Gwet's agreement coefficient
Acc	Accuracy
BVC	Best valuable comparator
CNR	Contrast-to-noise ratio
CRR	Contrast-to-reference ratio
CT TAP	Computed tomography of thorax, abdomen, and pelvis
DWI	Diffusion-weighted imaging
FF	Fat fraction
FN	False negative
FP	False positive
IP	In-phase imaging from the T2 Dixon sequence
MM	Multiple myeloma
OP	Out-of-phase imaging from the T2 Dixon sequence
PET	Positron emission tomography
ROI	Region of interest
Se	Sensitivity
SI	Signal intensity
SNR	Signal-to-noise ratio
Sp	Specificity
STIR	Short-Tau inversion recovery
TN	True negative
TP	True positive
TSE	Turbo spin echo
WB-MRI	Whole-body magnetic resonance imaging

Introduction

Over recent years, whole-body magnetic resonance imaging (WB-MRI) has demonstrated a high diagnostic performance and is now recommended in clinical guidelines for skeletal lesion detection and follow-up in patients with metastases from solid cancers and multiple myeloma (MM) [1–6]. Standard WB-MRI examinations combine anatomic T1 and short-Tau inversion recovery (STIR) sequences and functional diffusion-weighted imaging (DWI) sequences [7–9]. T1 is the reference sequence for marrow lesion detection and characterization; STIR increases the sensitivity for lesion detection [10, 11]. DWI sequences add diagnostic value to anatomic

sequences thanks to a high lesion to background contrast and extend cancer screening to lymph nodes and extraskelatal organs [12–16]. A limitation of WB-MRI is its duration and various initiatives are undertaken to accelerate the different sequences [17–19].

The Dixon technique relies on the chemical shift between protons of water and fat and decomposes the signal from these two components in the same voxel. A Dixon sequence generates four types of images: in-phase (IP) (equivalent to non-fat-suppressed anatomic images), out-of-phase (OP), water images (equivalent to fat-suppressed), and fat images (equivalent to water-suppressed) [20–22]. A single T2 Dixon sequence combines STIR-like information thanks to water images, and T1-like information thanks to fat images [23–25]. The diagnostic performance of the T2 Dixon sequence for detecting metastatic and MM lesions and its ability to replace the T1+STIR sequences has been demonstrated in spinal MRI examinations [26–28].

Herein, we hypothesized that a faster WB-MRI protocol using a single T2 Dixon sequence may be used without loss of diagnostic accuracy for detecting neoplastic bone marrow lesions. This study compares the (i) repeatability and reproducibility, (ii) image quality (signal-to-noise ratio (SNR); contrast-to-noise ratio (CNR); contrast-to-reference ratio (CRR), and (iii) diagnostic accuracy of combined fat + water reconstructions from a single T2 Dixon sequence with those of the combined T1+STIR sequences.

Materials and methods

Patient population (Fig. 1)

The study included consecutive adult (≥ 18 years old) patients with either solid cancers at high risk for metastases or biopsy-proven newly diagnosed multiple myeloma (MM).

The indication for WB-MRI in newly diagnosed patients with solid cancers was validated in multidisciplinary tumor boards using cancer-specific indications.

In prostate cancer, high risk for metastasis was defined according to the National Comprehensive Cancer Network (NCCN) guidelines: cancer with ≥ 20 ng/ml prostate-specific

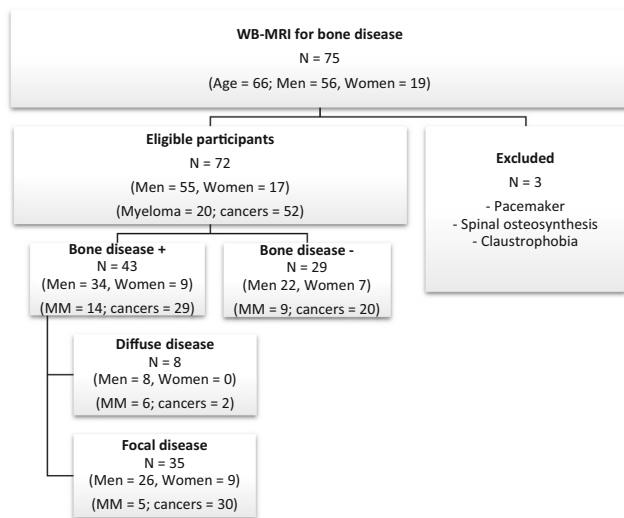


Fig. 1 Patient demographics

antigen, Gleason score ≥ 8 , and Union for International Cancer Control clinical T stage 3 or 4 [29]. In breast cancer, high risk was defined according to the European Society of Medical Oncology (ESMO) criteria: clinically positive axillary nodes, tumors > 5 cm, aggressive biology and clinical signs, and symptoms or laboratory values suggesting the presence of metastases [30]. In neuroendocrine cancer, high risk for metastasis was defined as follows: tumor grade \geq III, tumor size ≥ 3 cm in diameter, T4 stage, N1 stage, histology of neuroendocrine carcinoma, and esophagus as the primary site [31].

Exclusion criteria were previous history of treated cancer, patients with more than one primary cancer, and contraindications to MRI.

All patients underwent a WB-MRI examination for the assessment of bone involvement from January 2019 to January 2020. This single-center study was approved by the institutional ethics committee. No informed consent was required for the retrospective reading of prospectively acquired data.

MRI protocol

All acquisitions were performed on a 3.0-T magnet (Ingenia, Philips Healthcare). Patients were imaged head first in the supine position, from head to proximal femurs, covered with head, neck, spine, and two 6-element body matrix coils. 3DT1, STIR, T2 Dixon and DWI sequences were performed. Synthetic water, fat, IP, and OP images were automatically reconstructed from the Dixon acquisition. After acquiring three stacks of T1, STIR, and T2 Dixon images in the coronal plane and four stacks of DWI in the axial plane, a single stack of pasted reformatted coronal images was constructed for each sequence. The total acquisition time was 49 min. Imaging parameters are detailed in Table 1.

MRI readings

All images were stored and read on the institutional Picture Archiving and Communication System (Carestream Vue). The combinations of T1+STIR sequences and of fat+water reconstructions from the T2 Dixon sequence were assessed by two radiologists with 2- and 15-years' experience in WB-MRI. Readings were performed independently, randomly, and blinded to clinical information and to DWI. Images were assessed twice by the junior reader at a 3-month interval for measuring the repeatability. IP and OP images derived from the Dixon acquisition were not considered for analysis as they did not add diagnostic value for lesion detection based on preliminary evaluation and literature [26]. DWI was used during the consensus session for determining the reference standard.

Bone involvement

Four patterns of bone marrow involvement were considered, as previously described: the normal, focal, diffuse, and "salt-and-pepper" patterns [6, 12, 32–36].

Normal marrow was defined as showing a homogeneous high signal intensity on T1 and fat images, and homogeneous low signal intensity on STIR and water images. A focal bone marrow lesion (focal metastasis in solid cancers or focal plasmocytoma in MM, with a minimal diameter of 5 mm) was defined as a low signal intensity area on T1 and fat images (similar to or lower than the signal intensity of discs and muscles on T1, very low signal on fat), intermediate to high signal intensity on STIR and water images, and high signal intensity on high *b*-value DW images. Diffuse marrow infiltration (diffuse metastatic disease in solid cancers and diffuse bone involvement in MM) was defined as homogeneous low signal intensity of the bone marrow on T1 and fat images (similar to or lower than the signal intensity of discs and muscles on T1, very low signal on fat), an intermediate to high signal intensity of the marrow on STIR and water images, and high signal intensity of the marrow on high *b*-value images. The fourth "salt-and-pepper" pattern of infiltration was observed in MM, defined by the presence of innumerable unmeasurable tiny foci with low signal intensity on T1 and fat and intermediate to high signal intensity on STIR and water images.

Eight skeletal regions were studied: skull, thoracic cage, cervical, thoracic, lumbar spine, pelvis, humerus, and femurs. In the *per*-region analysis, two scores were assessed: a categorical score (presence of lesion = yes/no) and a semi-quantitative score corresponding to the count of lesions (0 = no lesion; 1 = 1 to 5 lesions; 2 = 6 to 10 lesions; 3 = more than 10 lesions; 4 = diffuse disease). In the *per*-patient analysis, two similar scores were assessed: a total categorical score (patient positive if at least one positive region = yes/

Table 1 Imaging parameters

Parameters	3D T1 FSE	T2 Dixon	STIR	DWI
Scan orientation	Coronal	Coronal	Coronal	Axial
Phase-encoding direction	feet-head	Left-right	Feet-head	Anterior-posterior
Acquired voxel size (mm) (read x phase x slice)	1.14 × 1.30 × 1.20	1.19 × 1.40 × 4	1.2 × 1.60 × 4	4.4 × 4.8 × 6
Field of view (mm) (read x phase x slice)	500 × 350 × 252	350 × 496 × 250	500 × 350 × 256	440 × 348 × 305
No. of stations	3	3	3	4
Overlap between stations (mm)	50	50	50	50
Coverage in z-axis (mm)	1050	1050	1050	1070
Phase oversampling (mm)	200 × 200	No	180×120	0
TR/TE (ms)	285 / 21	3722 / 55	7500 / 50	6000 / 59
TI (ms)	-	-	200	250
No. of signals acquired	2	1	2	1
Turbo factor	50	11	30	NA
Bandwidth (Hz)	1052	763	640	107
Fat suppression technique	-	Dixon	STIR	SPAIR
<i>b</i> values, s/mm ²	-	-	-	0-50-150-1000
Acquisition time, per stack	3 min 38 s	4 min 13 s	3 min 39 s	3 min 36 s
Total acquisition time, per sequence	3 × 3 min 38 s 10 min 54 s	3 × 4 min 13 s 12 min 39 s	3 × 3 min 39 s 10 min 57 s	4 × 3 min 36 s 14 min 24 s

Notes. FSE, fast spin-echo; STIR, short-TI inversion recovery sequence; DWI, diffusion-weighted imaging sequence; TR, repetition time; TE, echo time; TI, inversion time

no) and a total semi-quantitative score corresponding to the total count of lesions in all regions considered (0 = no lesion; 1 = 1 to 5 lesions; 2 = 6 to 10 lesions; 3 = more than 10 lesions; 4 = diffuse disease).

Reference standard and adjudication of readings

In the absence of a systematic pathologic gold standard, a best valuable comparator (BVC) was used as the reference standard for tumoral bone marrow involvement. This BVC was constructed during a consensus session by the readers along with a third reader (radiologist with 15 years' experience in WB-MRI) and clinicians, relying on the concurrent study of all baseline WB-MRI sequences (T1, STIR, T2 fat and water, DWI), clinical data, and other available imaging studies [37, 38]. At least one systematic 6-month follow-up WB-MRI examination was performed in all patients. A radiographic skeletal survey was performed at diagnosis and repeated after 6 months in all MM patients. In solid cancer patients, baseline and follow-up evaluations using other techniques (bone scintigraphy, thoraco-abdomino-pelvic (TAP) CT, positron-emission tomography (PET)-CT) were available, depending on the primary cancer. The causes of false positive (FP) / false negative (FN) were determined for each protocol and reader during the consensus session.

Image quality

As the value of an imaging sequence used for lesion detection depends on the contrast between lesions and their environment, SNR ($SNR = SI / \sigma_{\text{background}}$), CNR ($CNR = (SI^{\text{lesion}} - SI^{\text{reference}}) / \sigma_{\text{background}}$), and CRR ($CRR = (SI^{\text{lesion}} - SI^{\text{reference}}) / SI^{\text{reference}}$) were assessed (SI: mean signal intensity in the region of interest (ROI), $\sigma_{\text{background}}$: standard deviation of SI in the image background). Measurements were performed by the junior reader after verification of the true pathologic nature of the measured lesions according to the reference standard. A single ROI, the largest possible, was drawn within bone lesions without including bone cortices, with a maximum of five lesions per patient and a minimal diameter of 10 mm. For spine lesions, the reference ROI was chosen in an unequivocally non-involved bone marrow area of the involved vertebra or in case of large lesions in the bone marrow of the closest uninvolved vertebra. For other bone lesions, the reference ROI was chosen in an unequivocally non-involved area. Two ROIs, the largest possible, were drawn in the image background to assess the noise. All measurements were performed on the same coronal slice.

Statistical analysis

Due to the non-normality of data distributions (according to the Shapiro-Wilk test at $p < 0.05$), the comparison of SNR,

CNR, and CRR measurements between protocols was performed using Wilcoxon's signed-rank test [39].

Repeatability and reproducibility of MRI (categorical and semi-quantitative) scores were assessed using Gwet's AC1 agreement coefficient [40]. Strength of intra-(repeatability) and inter-reader agreement (reproducibility) was interpreted according to the Landis-Koch's scale: $AC1 < 0.20$ = poor; $0.21 \leq AC1 < 0.40$ = fair; $0.41 \leq AC1 < 0.60$ = moderate; $0.61 \leq AC1 < 0.80$ = good and $AC1 \geq 0.81$ = very good [41].

Diagnostic characteristics and agreement between each protocol and the reference standard were assessed. True positives (TP), false positives (FP), false negatives (FN), true negatives (TN), sensitivity (Se), specificity (Sp), accuracy ($Acc = (TP + TN) / (TP + FP + FN + TN)$), and AC1 were reported for the *per-region/per-patient* analyses (for both readers). A two-sided exact test was used for comparing the proportion of lesions/patients correctly detected in the *per-region/per-patient* analyses by each protocol compared to the reference standard (significance level after Bonferroni-like correction $p < 0.0083$). This analysis was performed for the whole cohort of patients, and for two subgroups ($N = 20$ patients with MM and $N = 52$ patients with metastases; see [Supplementary Materials](#)).

Difference in Acc between protocols in the *per-patient* analysis was assessed using a resampling procedure (without replacement) based on 300 samples of $N = 54$ patients randomly drawn from the whole cohort of $N = 72$ patients (respectively based on samples of $N = 15/N = 38$ patients randomly drawn from the subgroups of patients with MM/metastases). A paired t-test was then performed from which the mean difference in Acc was reported for each of the three groups that were studied (significance level $p < 0.0083$; see [Supplementary Materials](#)).

Finally, an agreement between each protocol and the reference standard on the semi-quantitative score in the *per-patient* analysis was assessed using the AC1 coefficient.

All calculations were done with Statsdirect Statistical Software v3.3.5 and with Matlab R2021b.

Results

Patient characteristics

Seventy-two patients were included (55 men, 17 women, median age = 66 years [64 years; 68 years]). Twenty were examined for staging biopsy-proven MM. Fifty-two had newly diagnosed solid cancers at high risk for metastases (30 prostate cancers; 10 breast cancers; 12 neuroendocrine cancers) (Fig. 1). According to the reference standard, 35 (5 MM; 30 solid cancer patients) had focal bone lesions; 8 (6 MM; 2 solid cancer patients) had diffuse marrow involvement; and 29 had normal marrow (9 MM; 20 solid

cancer patients). Due to the semi-quantitative scoring, the exact number of focal lesions cannot be provided. There were at least 3, 91, 26, 80, 64, 220, 8, and 27 focal lesions in the skull, thorax, cervical, dorsal, lumbar spine, pelvis, humerus, and femurs, respectively; in total, at least 519 tumoral bone marrow lesions were observed.

Repeatability and reproducibility

In the *per-region* analysis, repeatability of readings was at least good regardless of the region, score (categorical or semi-quantitative), and protocol (T1+STIR or fat+water) (Table 2). Reproducibility was at least good regardless of the region, score, and protocol. In the *per-patient* analysis, considering the worst level of agreement measured in both analyses (intra- and inter-reader agreement), reproducibility was at least good regardless of both the score and protocol.

Image quality

T1 images had significantly higher SNR compared to T2 Dixon fat images for both tissue types ($p^{\text{lesion}} < 0.0001$; $p^{\text{reference}} < 0.0093$). T2 Dixon fat images had significantly higher CRR compared to T1 images ($p < 0.0001$), and T2 Dixon water images had a significantly higher CRR compared to STIR images ($p = 0.0128$) (Table 3).

Diagnostic characteristics

In the *per-region* analysis, Se of T1+STIR was $\geq 93\%$ for the senior reader ($\geq 89\%$ for the junior) regardless of the region (Table 4). Sp was $\geq 94\%$ for the senior reader ($\geq 82\%$ for the junior) regardless of the region. Se of T2 Dixon fat+water was $\geq 93\%$ for the senior reader ($\geq 93\%$ for the junior) regardless of the region. Sp was $\geq 91\%$ for the senior reader ($\geq 75\%$ for the junior).

In the *per-patient* analysis, two trends were observed. First, the junior reader achieved a similar Se but a lower Sp compared to the senior, regardless of the protocol. Second, the senior reader achieved a slightly higher Se with the T2 Dixon protocol (Se = 98% vs Se = 93% with T1+STIR) while the junior achieved a slightly lower Sp with that protocol (Sp = 72% vs Sp = 79% with T1+STIR).

Compared to the reference standard, no significant difference was observed in the proportion of lesions correctly detected in the *per-region* analysis, or in the proportion of positive patients correctly detected in the *per-patient* analysis, regardless of both the reader and protocol (Figs. 2 and 3). A non-significant trend suggesting that the junior reader detected more humeral lesions (corresponding to FP) using T1+STIR compared to the reference standard was observed (proportion difference +8.33% [+ 1.28%; + 15.9%], $p = 0.0313$).

Table 2 Repeatability and reproducibility of MRI readings assessed using Gwet’s AC1 coefficient

	Reproducibility		Repeatability	
	Inter-reader agreement		Intra-reader agreement	
Categorical score = positive yes/no				
	T1+STIR	Fat + water	T1+STIR	Fat + water
Skull	0.98 [0.94; 1.02]	0.98 [0.94; 1.02]	0.96 [0.91; 1.01]	0.98 [0.94; 1.02]
Thorax	0.90 [0.80; 1.00]	0.95 [0.88; 1.02]	0.83 [0.70; 0.95]	0.83 [0.70; 0.95]
Cervical spine	0.92 [0.84; 1.00]	0.98 [0.94; 1.02]	0.88 [0.78; 0.98]	0.96 [0.91; 1.02]
Thoracic spine	0.87 [0.75; 0.98]	0.89 [0.79; 1.00]	0.87 [0.75; 0.94]	0.87 [0.75; 0.98]
Lumbar spine	0.76 [0.61; 0.91]	0.97 [0.92; 1.02]	0.76 [0.61; 0.91]	0.89 [0.79; 1.00]
Pelvis	0.84 [0.71; 0.96]	0.84 [0.72; 0.96]	0.67 [0.50; 0.84]	0.78 [0.64; 0.93]
Humerus	0.91 [0.83; 1.00]	0.94 [0.87; 1.01]	0.85 [0.74; 0.96]	0.92 [0.84; 1.00]
Femurs	0.88 [0.78; 0.98]	0.90 [0.81; 1.00]	0.78 [0.65; 0.92]	0.88 [0.77; 0.98]
<i>Per-patient</i>	0.82 [0.68; 0.95]	0.82 [0.69; 0.95]	0.74 [0.58; 0.89]	0.85 [0.72; 0.97]
Semi-quantitative score = count of lesions				
	T1+STIR	Fat + water	T1+STIR	Fat + water
Skull	0.98 [0.95; 1.02]	0.98 [0.95; 1.02]	0.97 [0.92; 1.01]	0.98 [0.95; 1.02]
Thorax	0.93 [0.87; 1.00]	0.97 [0.92; 1.01]	0.88 [0.80; 0.97]	0.88 [0.80; 0.97]
Cervical spine	0.92 [0.85; 0.99]	0.98 [0.95; 1.01]	0.91 [0.83; 0.98]	0.97 [0.93; 1.01]
Thoracic spine	0.90 [0.82; 0.98]	0.92 [0.85; 0.99]	0.91 [0.84; 0.99]	0.89 [0.81; 0.97]
Lumbar spine	0.82 [0.72; 0.92]	0.95 [0.90; 1.01]	0.82 [0.72; 0.92]	0.89 [0.81; 0.97]
Pelvis	0.85 [0.76; 0.94]	0.88 [0.80; 0.97]	0.77 [0.66; 0.88]	0.78 [0.68; 0.89]
Humerus	0.93 [0.86; 1.00]	0.95 [0.89; 1.01]	0.88 [0.80; 0.97]	0.93 [0.87; 1.00]
Femurs	0.92 [0.85; 0.99]	0.93 [0.87; 1.00]	0.82 [0.72; 0.92]	0.90 [0.82; 0.98]
<i>Per-patient</i>	0.76 [0.65; 0.87]	0.83 [0.73; 0.93]	0.71 [0.59; 0.83]	0.78 [0.67; 0.89]

In the *per-patient* analysis, the resampling procedure demonstrated a significantly higher Acc of T2 Dixon fat+water compared to T1+STIR when assessed by the senior reader (Acc^{Dixon Fat+Water} = 0.957, Acc^{T1+STIR} = 0.930, mean difference in Acc = +0.027 [+ 0.025; + 0.029], *p* < 0.0001). Conversely, it demonstrated a significantly lower Acc of T2 Dixon fat+water compared to T1+

STIR when assessed by the junior (Acc^{Dixon Fat+Water} = 0.860, Acc^{T1+STIR} = 0.889, mean difference in Acc = -0.029 [-0.031; -0.027], *p* < 0.0001).

When assessing differences in Acc according to the patient subgroups, the following observations were made (Supplementary Tables 1 and 2): the senior reader demonstrated a slightly higher Acc using the T2 Dixon protocol in the

Table 3 Image quality evaluation using SNR (signal-to-noise ratio), CNR (contrast-to-noise ratio), and CRR (contrast-to-reference ratio)

SNR	T1	STIR	Fat Dixon	Water Dixon	<i>p</i> value of the comparison	
					T1 vs fat Dixon	STIR vs water Dixon
Lesion	184 [136; 258]	144 [113; 252]	77.4 [57.9; 94.1]	142 [119; 202]	< 0.0001	0.3388
Reference	346 [268; 493]	98.5 [64.4; 188]	272 [207; 301]	71 [63; 96]	0.0093	0.0687
CNR	T1	STIR	Fat Dixon	Water Dixon	<i>p</i> value of the comparison	
					T1 vs fat Dixon	STIR vs water Dixon
(Lesion - Reference)/σ	160 [117; 201]	73.8 [49.7; 96.6]	179 [135; 227]	72.1 [52.6; 98.7]	0.6876	0.8518
CRR	T1	STIR	Fat Dixon	Water Dixon	<i>p</i> value of the comparison	
					T1 vs fat Dixon	STIR vs water Dixon
(Lesion - Reference)/reference	0.49 [0.39; 0.53]	0.78 [0.58; 0.97]	0.68 [0.65; 0.75]	0.95 [0.81; 1.12]	< 0.0001	0.0128

Note: σ= noise

SNR in the lesion and in the reference tissue, CNR (taking fat as reference), and CRR (ratio between lesion and reference tissue) measurements are provided. Median values and [95% confidence intervals] are reported. Significance threshold of the 2-sided Wilcoxon test: *p* < 0.05

Table 4 Diagnostic characteristics and agreement between the protocols and the Reference Standard in the whole cohort of patients ($N = 72$)

	TP	FP	FN	TN	Se	Sp	Acc	AC1	Proportion Difference (in %)	p value
Standard (3D T1 + STIR)										
Skull	11	1	0	60	100 [72; 100]	98 [91; 100]	99 [93; 100]	0.98 [0.94; 1.02]	-	> 0.9999
	11	0	0	61	100 [72; 100]	100 [94; 100]	100 [95; 100]	1.00 [1.00; 1.00]	-	> 0.9999
Thorax	21	5	1	45	95 [77; 100]	90 [78; 97]	92 [83; 97]	0.85 [0.73; 0.97]	-	0.2188
	21	1	1	49	95 [77; 100]	98 [89; 100]	97 [90; 100]	0.95 [0.88; 1.02]	-	> 0.9999
Cervical spine	12	4	0	56	100 [74; 100]	93 [84; 98]	94 [86; 98]	0.92 [0.84; 1.00]	-	0.1250
	12	0	0	60	100 [74; 100]	100 [94; 100]	100 [95; 100]	1.00 [1.00; 1.00]	-	> 0.9999
Thoracic spine	25	5	1	41	96 [80; 100]	89 [76; 96]	92 [83; 97]	0.84 [0.72; 0.96]	-	0.2188
	26	1	0	45	100 [87; 100]	98 [89; 100]	99 [93; 100]	0.97 [0.92; 1.02]	-	> 0.9999
Lumbar spine	24	8	3	37	89 [71; 98]	82 [68; 92]	85 [74; 92]	0.70 [0.54; 0.87]	-	0.2266
	26	1	1	44	96 [81; 100]	98 [88; 100]	97 [90; 100]	0.95 [0.88; 1.02]	-	> 0.9999
Pelvis	38	5	2	27	95 [83; 99]	84 [67; 95]	90 [81; 96]	0.81 [0.68; 0.94]	-	0.4531
	37	2	3	30	93 [80; 98]	94 [79; 99]	93 [85; 98]	0.86 [0.75; 0.98]	-	> 0.9999
Humeri	13	6	0	53	100 [75; 100]	90 [79; 96]	92 [83; 97]	0.87 [0.77; 0.98]	+ 0.08 [+ 0.01; + 0.16]	0.0313*
	13	2	0	57	100 [75; 100]	97 [88; 100]	97 [90; 100]	0.96 [0.90; 1.02]	-	0.5000
Femurs	19	5	1	47	95 [75; 100]	90 [79; 97]	92 [83; 97]	0.86 [0.74; 0.97]	-	0.2188
	19	0	1	52	95 [75; 100]	100 [93; 100]	99 [93; 100]	0.98 [0.93; 1.02]	-	> 0.9999
Per-patient	41	6	2	23	95 [84; 99]	79 [60; 92]	89 [79; 95]	0.79 [0.65; 0.93]	-	0.2891
	40	2	3	27	93 [81; 99]	93 [77; 99]	93 [85; 98]	0.87 [0.75; 0.98]	-	> 0.9999
T2 Dixon (fat + water)										
Skull	11	1	0	60	100 [72; 100]	98 [91; 100]	99 [93; 100]	0.98 [0.94; 1.02]	-	> 0.9999
	11	0	0	61	100 [72; 100]	100 [94; 100]	100 [95; 100]	1.00 [1.00; 1.00]	-	> 0.9999
Thorax	21	4	1	46	95 [77; 100]	92 [81; 98]	93 [85; 98]	0.88 [0.77; 0.98]	-	0.3750
	21	2	1	48	95 [77; 100]	96 [86; 100]	96 [88; 99]	0.93 [0.84; 1.01]	-	> 0.9999
Cervical spine	12	1	0	59	100 [74; 100]	98 [91; 100]	99 [93; 100]	0.98 [0.94; 1.02]	-	> 0.9999
	12	0	0	60	100 [74; 100]	100 [94; 100]	100 [95; 100]	1.00 [1.00; 1.00]	-	> 0.9999
Thoracic spine	25	7	1	39	96 [80; 100]	85 [71; 94]	89 [79; 95]	0.79 [0.64; 0.93]	-	0.0703
	25	3	1	43	96 [80; 100]	93 [82; 99]	94 [86; 98]	0.90 [0.79; 1.00]	-	0.6250
Lumbar spine	25	5	2	40	93 [76; 99]	89 [76; 96]	90 [81; 96]	0.81 [0.68; 0.95]	-	0.4531
	29	0	0	43	93 [76; 99]	91 [79; 98]	100 [95; 100]	0.84 [0.72; 0.96]	-	> 0.9999
Pelvis	38	8	2	24	95 [83; 99]	75 [57; 89]	86 [76; 93]	0.73 [0.58; 0.89]	-	0.1094
	39	3	1	29	98 [87; 100]	91 [75; 98]	94 [86; 98]	0.89 [0.79; 1.00]	-	0.6250
Humeri	13	3	0	56	100 [75; 100]	95 [86; 99]	96 [88; 99]	0.94 [0.87; 1.01]	-	0.2500
	13	0	0	59	100 [75; 100]	100 [94; 100]	100 [95; 100]	1.00 [1.00; 1.00]	-	> 0.9999
Femurs	20	4	0	48	100 [83; 100]	92 [82; 98]	94 [86; 98]	0.90 [0.81; 1.00]	-	0.1250
	20	0	0	52	100 [83; 100]	100 [93; 100]	100 [95; 100]	1.00 [1.00; 1.00]	-	> 0.9999
Per-patient	41	8	2	21	95 [84; 99]	72 [53; 87]	86 [76; 93]	0.74 [0.59; 0.90]	-	0.1094
	42	2	1	27	98 [88; 100]	93 [77; 99]	96 [88; 99]	0.92 [0.83; 1.01]	-	> 0.9999

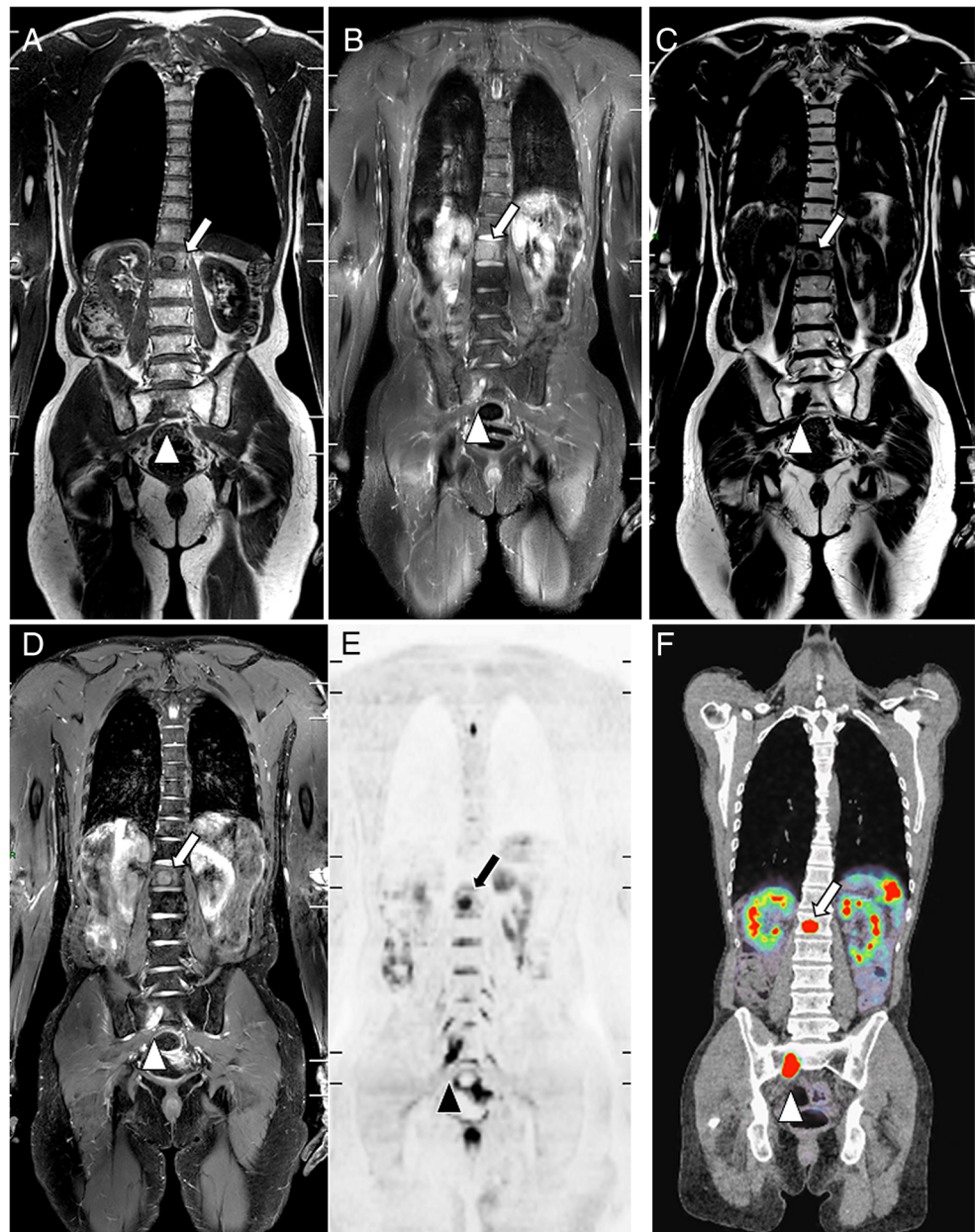
Notes: The difference in the proportion of lesions correctly detected in the *per*-region analysis, as well as the difference in the proportion of positive patients correctly detected in the *per*-patient analysis (both compared to the reference standard) is reported with the p value of the exact test. A single statistical difference (at $p < 0.05$ but not at $p < 0.0083$ after Bonferroni correction) is observed (*). Entries in boldface: junior reader; not in boldface: senior reader

TP true positive, *FP* false positive, *FN* false negative, *TN* true negative, *Se* sensitivity, *Spe* specificity, *Acc* accuracy, *AC1* Gwet's AC1 agreement coefficient

metastatic patient subgroup only (mean difference in $Acc = +0.036 [+ 0.033; + 0.038]$, $p < 0.0001$), while the junior reader demonstrated a slightly lower Acc using that protocol,

regardless of the patient subgroup (MM: mean difference in $Acc = -0.052 [-0.058; -0.046]$, $p < 0.0001$, metastatic patients: mean difference in $Acc = -0.019 [-0.021; -0.017]$, $p < 0.0001$).

Fig. 2 Agreement between sequences on metastatic lesions: WB-MRI study in a 46-year-old man with metastatic neuroendocrine cancer. Two metastases are observed in the L1 vertebral body (arrow) and in the right wing of the sacrum (arrowhead). Coronal T1 (A) and STIR (B) WB-MRI images show both lesions. Fat (C) and water (D) reconstructions of the TSE T2 Dixon acquisition show the same lesions. The reference standard, based on reading of all MR images and concurrent imaging studies, confirmed the presence of two metastases. E Concurrent DWI image ($b = 1000 \text{ s mm}^{-2}$, inverted gray scale) confirms the presence of both lesions and shows no additional lesion. F Gallium-68 dotatate PET/CT fused image shows the same two lesions presenting tracer uptake



Semi-quantitative score

In the *per*-patient analysis, agreement between the protocols and the reference standard was good for the junior reader (regardless of the protocol), and very good for the senior reader (regardless of the protocol) (T1+STIR vs reference standard: $AC1^{\text{junior}} = 0.76$ [0.65; 0.87], $AC1^{\text{senior}} = 0.86$ [0.77; 0.95]; T2 Dixon fat+water vs reference standard: $AC1^{\text{junior}} = 0.78$ [0.68; 0.89], $AC1^{\text{senior}} = 0.93$ [0.87; 1.00]).

False-negative and false-positive readings

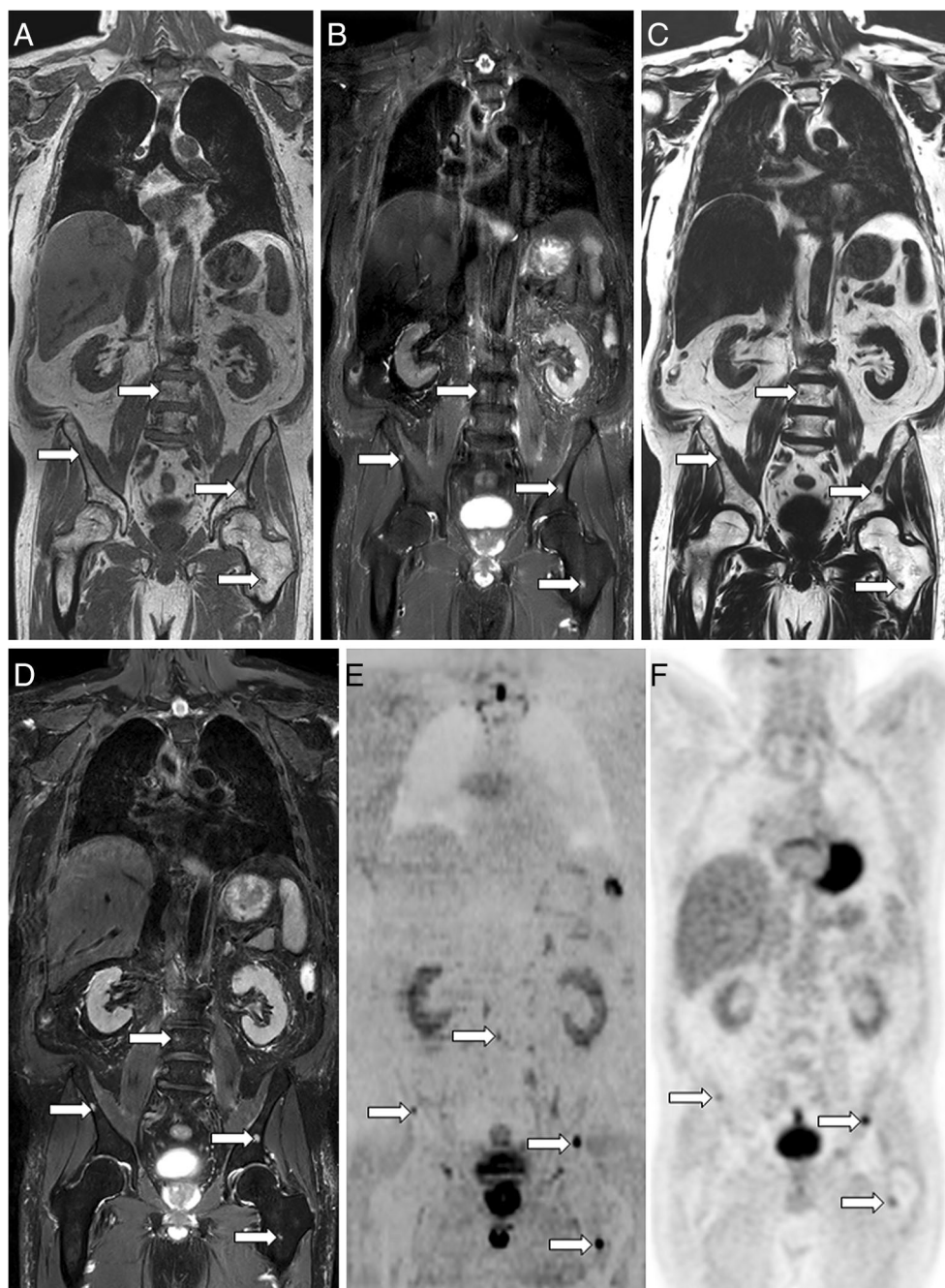
FP readings resulted from benign conditions: degenerative disease (subchondral cysts, juxta-articular/discal changes),

enchondromas, focal marrow hyperplasia, vertebral hemangiomas, enostosis, and benign fractures. FN readings resulted from missed lesions (Table 5) (Fig. 4).

Discussion

This study compared the diagnostic accuracy of a single T2 Dixon sequence including fat+water reconstructions to the guidelines-recommended combination of T1+STIR sequences used as morphological sequences in WB-MRI examinations performed to detect skeletal metastases or MM lesions [7–9]. Our results showed that the accuracy (Acc) of the combination of T2 Dixon fat+water reconstructions was

Fig. 3 Agreement between sequences on myeloma lesions: WB-MRI study in a 65-year-old man with newly diagnosed multiple myeloma. Several lesions are observed in the lumbar spine, iliac bones, and left femur (arrows). Coronal T1 (A) and STIR (B) WB-MRI images show four lesions. Fat (C) and water (D) reconstructions of the TSE T2 Dixon acquisition show the same lesions. The reference standard, based on reading of all MR images and concurrent imaging studies, confirmed the presence of these lesions. E Concurrent DWI image ($b = 1000 \text{ s mm}^{-2}$, inverted gray scale) confirms the presence of lesions. F ^{18}F -FDG PET/CT image shows iliac and left femur lesions presenting tracer uptake



similar (-2.9% ; $+2.7\%$) to that of the reference protocol combining T1+STIR sequences.

These results are in line with published studies that compared the performance of a T2 Dixon sequence and of the combination of T1 and fat-suppressed fluid-sensitive sequences in MRI studies limited to the spine or to a spine segment for the detection of metastases or MM [26–28]. These three studies concluded that the T2 Dixon protocol had similar diagnostic performance compared to the standard protocol, providing STIR-like (fluid sensitive) information

with the water image, and T1-like (fat sensitive) information with the fat image, and that its use significantly reduces the acquisition time of spine MRI in oncologic indications.

The present study extends this conclusion to WB-MRI examinations used for skeletal screening.

Both repeatability and reproducibility of readings were at least good for both the T2 Dixon and the T1+STIR protocols, for both the categorical (disease present/absent) and semi-quantitative scores (lesion count), and in both the regional and global (*per-patient*) analyses. Of note, all quantitative

Table 5 Analysis of the false-positive and false-negative findings, as determined during the consensus adjudication

False-positive findings	Junior reader		Senior reader	
	<i>N</i>	Cause	<i>N</i>	Cause
Standard (T1+STIR)				
	3	Focal marrow hyperplasia	2	Focal marrow hyperplasia
	7	Degenerative	1	Degenerative
	2	Enchondroma	0	Enchondroma
	3	Angioma	1	Angioma
	1	Enostosis	0	Enostosis
	2	Benign fracture	2	Benign fracture
T2 Dixon fat+water				
	2	Hematopoiesis	2	Hematopoiesis
	6	Degenerative	0	Degenerative
	2	Enchondroma	0	Enchondroma
	4	Angioma	1	Angioma
	2	Enostosis	1	Enostosis
	3	Benign fracture	2	Benign fracture
False-negative findings	<i>N</i>	Cause	<i>N</i>	Cause
Standard (T1+STIR)				
	3	Thoracic	0	Thoracic
	2	Lumbar	0	Lumbar
	9	Pelvis	3	Pelvis
T2 Dixon fat+water				
	3	Thoracic	3	Thoracic
	2	Lumbar	2	Lumbar
	9	Pelvis	8	Pelvis

False-positive observations are benign conditions considered malignant

False-negative observations are missed lesions; the anatomic location of these false-negative lesions is indicated

evaluations of repeatability/reproducibility (Gwet's coefficient) were higher for the T2 Dixon evaluation compared to T1+STIR.

Regarding image quality, the T1 sequence had higher SNR compared to the T2 Dixon fat images in lesions and reference areas. This difference is not unexpected as the T1 sequence is acquired in 3D mode, which intrinsically provides a higher signal than 2D sequences [42]. This differs from the studies of Maeder and Danner, where a higher SNR for the T2 Dixon fat images compared to the T1 images acquired in 2D mode was found [26, 28]. In our study, the T1 and the T2 Dixon fat sequences had similar CNR. Interestingly, T2 Dixon fat images had significantly higher CRR compared to T1 images, and T2 Dixon water images had significantly higher CRR compared to STIR images. In practice, this higher CRR results in an improved detectability of the lesions.

Regarding the diagnostic performance, both protocols showed similar levels of sensitivity and specificity in the *per*-region analysis, with no significant difference between them in the proportion of correctly detected lesions, compared to the reference standard. Some FP and FN findings were

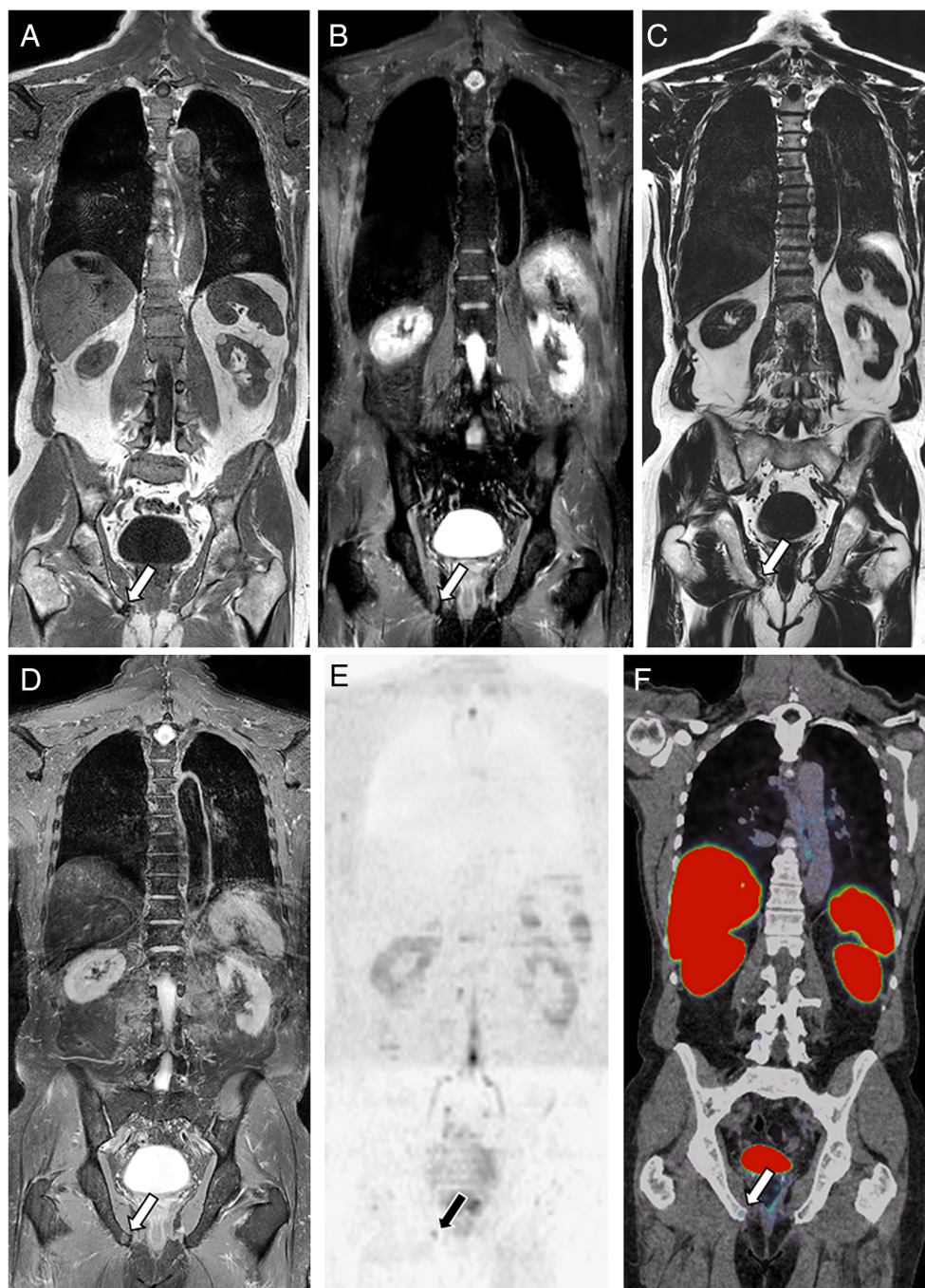
observed, presenting similar causes for both protocols and both readers.

The junior reader had a higher number of FP observations compared to the senior, resulting in a lower specificity and accuracy, in both the *per*-region and *per*-patient analyses. FP observations were errors of interpretation of degenerative changes or benign conditions, already reported as pitfalls in previous studies of the diagnostic performance of WB-MRI for the detection of bone marrow lesions [11, 43]. These causes of FP should be taken into account during the learning phase of less-experienced readers to avoid overdiagnosis.

Both readers had a low number of FN observations, leading to high sensitivity of both the T2 Dixon and T1+STIR protocols. FNs were due to errors of detection, i.e. lesions missed by the reader or lesions not seen on the available sequences but detected by the reference standard.

Considering the high level of accuracy achieved in this study and the shorter acquisition time, the T2 Dixon protocol represents a realistic alternative to the classical T1+STIR combination for the skeletal screening and follow-up of patients with metastases from solid cancers and MM. In our center, its implementation allows sparing

Fig. 4 False-negative observation (detection error): WB-MRI in a 71-year-old man with newly diagnosed prostate cancer. Coronal T1 (A) and STIR (B) WB-MRI images show single centimetric bone metastasis within the right ischio-pubic ramus, with low signal intensity on T1 and high signal intensity on STIR (arrow). The lesion was missed by one observer on these T1 and STIR images. Fat (C) and water (D) reconstructions of the T2 Dixon acquisition show the same lesion with low signal intensity on the FAT image and high signal intensity on the WATER image (arrows). The reference standard, based on reading of all MR images and concurrent imaging studies, confirmed the presence of a solitary right ischio-pubic lesion. E Concurrent DWI image ($b = 1000 \text{ s mm}^{-2}$, inverted gray scale) confirms the presence of the lesion (arrow). F Gallium-68 PSMA fused PET/CT image confirms the presence of the lesion



9 min 12s in the acquisition time of morphological sequences. The total acquisition time of WB-MRI including T2 Dixon and DWI sequences is 27 min 03 s.

This study has several limitations. First, it was performed in a single center and on a single MRI magnet. However, the cohort of patients was large and representative of current WB-MRI indications. Enlarging the cohort of patients should allow refining the evaluation of the difference in accuracy between protocols. Extending our protocol in a multi-centric study including patients imaged on different MRI magnets

and multiple readings should allow the generalization of our observations.

Second, only the fat and water reconstructions derived from the T2 Dixon sequence were used, excluding IP and OP images. This choice relies on previous observations showing the lack of added value of IP and OP images to detect bone lesions [26]. However, the availability of IP and OP images may be an additional advantage of the T2 Dixon protocol. Indeed, IP images are equivalent to non-fat-suppressed T2-weighted images and provide anatomic information that may

be useful in the evaluation of the spinal canal and spinal cord, in the characterization of vertebral fractures, and in the detection of visceral and lymph node metastases without additional imaging time [44]. Moreover, the availability of IP and OP images and their comparisons may help in the determination of the neoplastic nature of an ambiguous bone marrow lesion and in the recognition of focal marrow hyperplasia and acute benign vertebral fractures, which are frequent pitfalls causing FP observations. Benign lesions indeed show a signal dropout on OP images due to the intravoxel coexistence of microscopic fatty components and hydrated normal cells within the bone marrow [45, 46]. Besides this qualitative approach, the T2 Dixon sequence allows fat fraction (FF) quantification, which can be used to differentiate benign and malignant lesions [24]. Further studies should assess the added value of IP and OP images and of FF measurements.

Third, this study only assessed the diagnostic performance of morphological sequences, in a time-saving perspective. Although the DWI sequence was systematically available, we did not compare its diagnostic accuracy to that of anatomic sequences. The high accuracy (close to 1.00) of the T2 Dixon fat+water protocol suggests that this morphologic sequence alone may be sufficient for skeletal screening, with no need for DWI. This high performance of the anatomic T2 Dixon for bone screening, making DWI superfluous in this indication, has been suggested in a study in 5 patients with bone metastases of renal cancer [47]. We did not question the recommended systematic combination of anatomic and functional DWI sequences. Indeed, DWI sequences allow optimization of bone lesion detection, screening of lymph nodes and visceral lesions, and provide ADC measurements useful for lesion characterization and assessment of treatment response [7, 9, 48–50].

Conclusion

This study in patients with bone metastases or MM shows that a shorter anatomical WB-MRI protocol relying on a single T2 Dixon sequence with fat and water reconstructions may replace the reference T1+STIR sequences for skeletal screening, shortening examination duration, without loss of diagnostic accuracy.

Supplementary Information The online version contains supplementary material available at <https://doi.org/10.1007/s00330-022-09007-8>.

Funding The authors state that this work has not received any funding.

Declaration

Guarantor The scientific guarantor of this publication is Frederic E. Lecouvet.

Conflict of interest The authors of this manuscript declare no relationships with any companies, whose products or services may be related to the subject matter of the article.

Statistics and biometry One of the authors (Nicolas Michoux) has significant statistical expertise.

Informed consent Written informed consent was waived by the Institutional Review Board.

Ethical approval Institutional Review Board approval was obtained.

Methodology

- retrospective
- cross-sectional study
- performed at one institution

Open Access This article is licensed under a Creative Commons Attribution 4.0 International License, which permits use, sharing, adaptation, distribution and reproduction in any medium or format, as long as you give appropriate credit to the original author(s) and the source, provide a link to the Creative Commons licence, and indicate if changes were made. The images or other third party material in this article are included in the article's Creative Commons licence, unless indicated otherwise in a credit line to the material. If material is not included in the article's Creative Commons licence and your intended use is not permitted by statutory regulation or exceeds the permitted use, you will need to obtain permission directly from the copyright holder. To view a copy of this licence, visit <http://creativecommons.org/licenses/by/4.0/>.

References

1. Lauenstein TC, Goehde SC, Herborn CU et al (2004) Whole-body MR imaging: evaluation of patients for metastases. *Radiology* 233: 139–148
2. Walker R, Kassar P, Blanchard R et al (2000) Turbo STIR magnetic resonance imaging as a whole-body screening tool for metastases in patients with breast carcinoma: preliminary clinical experience. *J Magn Reson Imaging* 11:343–350
3. Kwee TC, Kwee RM, Verdonck LF, Bierings MB, Nievelstein RA (2008) Magnetic resonance imaging for the detection of bone marrow involvement in malignant lymphoma. *Br J Haematol* 141:60–68
4. Ghanem N, Lohrmann C, Engelhardt M et al (2006) Whole-body MRI in the detection of bone marrow infiltration in patients with plasma cell neoplasms in comparison to the radiological skeletal survey. *Eur Radiol* 16:1005–1014
5. Dimopoulos MA, Hillengass J, Usmani S et al (2015) Role of magnetic resonance imaging in the management of patients with multiple myeloma: a consensus statement. *J Clin Oncol* 33:657–664
6. Lecouvet FE, Boyadzhiev D, Collette L et al (2019) MRI versus [¹⁸F]F-FDG-PET/CT for detecting bone marrow involvement in multiple myeloma: diagnostic performance and clinical relevance. *Eur Radiol*. <https://doi.org/10.1007/s00330-019-06469-1>
7. Padhani AR, Lecouvet FE, Tunariu N et al (2017) METastasis reporting and data system for prostate cancer: practical guidelines for acquisition, interpretation, and reporting of whole-body magnetic resonance imaging-based evaluations of multiorgan involvement in advanced prostate cancer. *Eur Urol* 71:81–92

8. Messiou C, Hillengass J, Delorme S et al (2019) Guidelines for acquisition, interpretation, and reporting of whole-body MRI in myeloma: Myeloma Response Assessment and Diagnosis System (MY-RADS). *Radiology* 291:5–13
9. Lecouvet FE (2016) Whole-body MR imaging: musculoskeletal applications. *Radiology* 279:345–365
10. Mirowitz SA, Apicella P, Reinus WR, Hammerman AM (1994) MR imaging of bone marrow lesions: relative conspicuousness on T1-weighted, fat-suppressed T2-weighted, and STIR images. *AJR Am J Roentgenol* 162:215–221
11. Larbi A, Omoumi P, Pasoglou V et al (2019) Whole-body MRI to assess bone involvement in prostate cancer and multiple myeloma: comparison of the diagnostic accuracies of the T1, short tau inversion recovery (STIR), and high b-values diffusion-weighted imaging (DWI) sequences. *Eur Radiol* 29:4503–4513
12. Padhani AR, Koh DM, Collins DJ (2011) Whole-body diffusion-weighted MR imaging in cancer: current status and research directions. *Radiology* 261:700–718
13. Takenaka D, Ohno Y, Matsumoto K et al (2009) Detection of bone metastases in non-small cell lung cancer patients: comparison of whole-body diffusion-weighted imaging (DWI), whole-body MR imaging without and with DWI, whole-body FDG-PET/CT, and bone scintigraphy. *J Magn Reson Imaging* 30:298–308
14. Takahara T, Imai Y, Yamashita T, Yasuda S, Nasu S, Van Cauteren M (2004) Diffusion weighted whole body imaging with background body signal suppression (DWIBS): technical improvement using free breathing, STIR and high resolution 3D display. *Radiat Med* 22:275–282
15. Pearce T, Philip S, Brown J, Koh DM, Burn PR (2012) Bone metastases from prostate, breast and multiple myeloma: differences in lesion conspicuity at short-tau inversion recovery and diffusion-weighted MRI. *Br J Radiol* 85:1102–1106
16. Sivesgaard K, Johnk ML, Larsen LP et al (2017) Comparison of four MRI protocols for detection of extrahepatic colorectal cancer metastases. *J Magn Reson Imaging* 46:1619–1630
17. Lecouvet FE, Pasoglou V, Van Nieuwenhove S et al (2020) Shortening the acquisition time of whole-body MRI: 3D T1 gradient echo Dixon vs fast spin echo for metastatic screening in prostate cancer. *Eur Radiol* 30:3083–3093
18. Zormpas-Petridis K, Tunariu N, Curcean A et al (2021) Accelerating whole-body diffusion-weighted MRI with deep learning-based denoising image filters. *Radiol Artif Intell* 3: e200279
19. Pasoglou V, Michoux N, Peeters F et al (2015) Whole-body 3D T1-weighted MR imaging in patients with prostate cancer: feasibility and evaluation in screening for metastatic disease. *Radiology* 275: 155–166
20. Dixon WT (1984) Simple proton spectroscopic imaging. *Radiology* 153:189–194
21. Ma J (2008) Dixon techniques for water and fat imaging. *J Magn Reson Imaging* 28:543–558
22. Bley TA, Wieben O, Francois CJ, Brittain JH, Reeder SB (2010) Fat and water magnetic resonance imaging. *J Magn Reson Imaging* 31:4–18
23. Zanchi F, Richard R, Hussami M, Monier A, Knebel JF, Omoumi P (2020) MRI of non-specific low back pain and/or lumbar radiculopathy: do we need T1 when using a sagittal T2-weighted Dixon sequence? *Eur Radiol* 30:2583–2593
24. Bacher S, Hajdu SD, Maeder Y, Dunet V, Hilbert T, Omoumi P (2021) Differentiation between benign and malignant vertebral compression fractures using qualitative and quantitative analysis of a single fast spin echo T2-weighted Dixon sequence. *Eur Radiol* 31:9418–9427
25. Guerini H, Omoumi P, Guichoux F et al (2015) Fat suppression with dixon techniques in musculoskeletal magnetic resonance imaging: a pictorial review. *Semin Musculoskelet Radiol* 19:335–347
26. Maeder Y, Dunet V, Richard R, Becce F, Omoumi P (2018) Bone marrow metastases: T2-weighted Dixon spin-echo fat images can replace T1-weighted spin-echo images. *Radiology* 286:948–959
27. Hahn S, Lee YH, Suh JS (2018) Detection of vertebral metastases: a comparison between the modified Dixon turbo spin echo T(2) weighted MRI and conventional T(1) weighted MRI: a preliminary study in a tertiary centre. *Br J Radiol* 91:20170782
28. Danner A, Brumpt E, Alilet M, Tio G, Omoumi P, Aubry S (2019) Improved contrast for myeloma focal lesions with T2-weighted Dixon images compared to T1-weighted images. *Diagn Interv Imaging* 100:513–519
29. Mohler JL, Kantoff PW, Armstrong AJ et al (2014) Prostate cancer, version 2.2014. *J Natl Compr Canc Netw* 12:686–718
30. Cardoso F, Paluch-Shimon S, Senkus E et al (2020) 5th ESO-ESMO international consensus guidelines for advanced breast cancer (ABC 5). *Ann Oncol* 31:1623–1649
31. Cai W, Tan Y, Ge W, Ding K, Hu H (2018) Pattern and risk factors for distant metastases in gastrointestinal neuroendocrine neoplasms: a population-based study. *Cancer Med* 7:2699–2709
32. Vanel D, Dromain C, Tardivon A (2000) MRI of bone marrow disorders. *Eur Radiol* 10:224–229
33. Baur-Melnyk A, Buhmann S, Durr HR, Reiser M (2005) Role of MRI for the diagnosis and prognosis of multiple myeloma. *Eur J Radiol* 55:56–63
34. Lecouvet FE, Simon M, Tombal B, Jamart J, Vande Berg BC, Simoni P (2010) Whole-body MRI (WB-MRI) versus axial skeleton MRI (AS-MRI) to detect and measure bone metastases in prostate cancer (PCa). *Eur Radiol* 20:2973–2982
35. Koh DM, Blackledge M, Padhani AR et al (2012) Whole-body diffusion-weighted MRI: tips, tricks, and pitfalls. *AJR Am J Roentgenol* 199:252–262
36. Mouloupoulos LA, Varma DG, Dimopoulos MA et al (1992) Multiple myeloma: spinal MR imaging in patients with untreated newly diagnosed disease. *Radiology* 185:833–840
37. Sanal SM, Flickinger FW, Caudell MJ, Sherry RM (1994) Detection of bone marrow involvement in breast cancer with magnetic resonance imaging. *J Clin Oncol* 12:1415–1421
38. Lecouvet FE, Geukens D, Stainier A et al (2007) Magnetic resonance imaging of the axial skeleton for detecting bone metastases in patients with high-risk prostate cancer: diagnostic and cost-effectiveness and comparison with current detection strategies. *J Clin Oncol* 25:3281–3287
39. Conover WJ (1999) *Practical Nonparametric Statistics*. John Wiley & Sons Inc., New York
40. Gwet KL (2008) Computing inter-rater reliability and its variance in the presence of high agreement. *Br J Math Stat Psychol* 61:29–48
41. Landis JR, Koch GG (1977) The measurement of observer agreement for categorical data. *Biometrics* 33:159–174
42. McRobbie DW, Moore EA, Graves MJ, Prince MR (2017) Acronyms anonymous. In: McRobbie DW, Moore EA, Graves MJ, Prince MR MRI from Picture to Proton. Cambridge University Press, pp 185–206
43. Ohno Y, Koyama H, Onishi Y et al (2008) Non-small cell lung cancer: whole-body MR examination for M-stage assessment—utility for whole-body diffusion-weighted imaging compared with integrated FDG PET/CT. *Radiology* 248:643–654
44. Low RN, Austin MJ, Ma J (2011) Fast spin-echo triple echo dixon: Initial clinical experience with a novel pulse sequence for simultaneous fat-suppressed and nonfat-suppressed T2-weighted spine magnetic resonance imaging. *J Magn Reson Imaging* 33:390–400
45. Douis H, Davies AM, Jeys L, Sian P (2016) Chemical shift MRI can aid in the diagnosis of indeterminate skeletal lesions of the spine. *Eur Radiol* 26:932–940
46. Zajick DC Jr, Morrison WB, Schweitzer ME, Parellada JA, Carrino JA (2005) Benign and malignant processes: normal values and

- differentiation with chemical shift MR imaging in vertebral marrow. *Radiology* 237:590–596
47. Wang X, Pirasteh A, Brugarolas J et al (2018) Whole-body MRI for metastatic cancer detection using T2 -weighted imaging with fat and fluid suppression. *Magn Reson Med* 80:1402–1415
 48. Giles SL, Messiou C, Collins DJ et al (2014) Whole-body diffusion-weighted MR imaging for assessment of treatment response in myeloma. *Radiology* 271:785–794
 49. Perez-Lopez R, Mateo J, Mossop H D et al (2017) Diffusion-weighted imaging as a treatment response biomarker for evaluating bone metastases in prostate cancer: a pilot study. *Radiology* 283:168–177
 50. Zhang L, Wang Q, Wu X et al (2021) Baseline bone marrow ADC value of diffusion-weighted MRI: a potential independent predictor for progression and death in patients with newly diagnosed multiple myeloma. *Eur Radiol* 31:1843–1852

Publisher's note Springer Nature remains neutral with regard to jurisdictional claims in published maps and institutional affiliations.